Superflexible Multifunctional Polyvinylpolydimethylsiloxane-Based Aerogels as Efficient Absorbents, Thermal Superinsulators, and Strain Sensors

Guoqing Zu, * [a] Kazuyoshi Kanamori, * [a] Ayaka Maeno, [b] Hironori Kaji, [b] and Kazuki Nakanishi [a]

Abstract: Aerogels are attractive porous materials but usually show poor mechanical properties and limited functionality, which significantly restrict their practical applications. Preparation of highly bendable and processable aerogels with multifunctionality still remains a difficult challenge. Here we report unprecedented superflexible aerogels based on polyvinylpolydimethylsiloxane (PVPDMS) network, PVPDMS/polyvinylpolymethylsiloxane (PVPMS) copolymer network, and PVPDMS/PVPMS/graphene nanocomposite via a facile radical polymerization/hydrolytic polycondensation strategy followed by low-cost ambient pressure drying or freeze drying. The resulting aerogels possess a doubly cross-linked organic-inorganic network structure consisting of flexible polydimethylsiloxanes and hydrocarbon chains with tunable cross-linking density, and exhibit tunable pore size and bulk density, high hydrophobicity, excellent processability, and superflexibility against both compression and bending. More importantly, they show multifunctionality combining selective absorption, efficient separation of oil and water, thermal superinsulation, and strain sensing. This study is expected to provide new concepts to synthesize multifunctional materials with a wide range of potential applications in absorbents, superinsulators, sensors, wearable electronics, etc.

Materials for environmental protection, energy saving, and smart sensing are increasingly needed to meet the growing social demands for sustainable development. [1-4] Porous materials including aerogels, [5,6] macroporous monoliths, [7] hydrogels, [8] polymer and carbon foams, [9] supramolecular gels, [10] metal-organic frameworks, [11] and periodic mesoporous materials[12] have drawn a lot of interest for their wide range of applications in thermal insulation, oil removal, energy storage, sensing, catalysis, drug delivery, etc. In particular, much attention has been paid to aerogels due to their unique properties such as high porosity, high specific surface area (SSA), low density, and low thermal conductivity. [13-15] So far, many kinds of aerogels based on silica, [16] metal oxide, [17,18] polymer, [19] carbon, [20] carbon nanotube, [21] and graphene[22] have been developed. However, traditional aerogels are usually dried via costly supercritical drying (SCD) and exhibit low mechanical strength because of their intrinsically fragile/brittle networks, which need to be addressed before their practical applications.

[a]   Dr. G. Zu, Prof. K. Kanamori, Prof. K. Nakanishi
        Department of Chemistry
        Graduate School of Science, Kyoto University
        Kitashirakawa, Sakyo-ku, Kyoto 606-8502 (Japan)
        E-mail: guoqingzu@icm.kuchem.kyoto-u.ac.jp (G. Zu),
        kanamori@kuchem.kyoto-u.ac.jp (K. Kanamori)
[b]   Dr. A. Maeno, Prof. H. Kaji
        Institute for Chemical Research, Kyoto University
        Gokasho, Uji, Kyoto 611-0011 (Japan)

        Supporting information for this article is given via a link at the end of the document.

In order to overcome the costly drying process and brittleness, many efforts have been made to lower the cost by ambient pressure drying (APD), [23] freeze drying (FD)[22] and vacuum drying (VD), [24] and reinforce the aerogels by a variety of methods. Cross-linking of aerogels with organic polymers is a widely used method to reinforce the aerogels but usually results in lower porosity and higher density that limit their applications. [25,26] Flexible polymer-based aerogels can be obtained from resorcinol-formaldehyde, [27] poly(vinyl alcohol), [28] and supramolecules, [29] and some of them exhibit good absorption of organic solvents/oils. Another kind of aerogels based on biomass such as nanocellulose and chitosan with compressibility and bendability have been reported. [30,31] Due to their highly porous nanostructure that is composed of nanofibers, they show excellent thermal insulation performances. Besides, assembly of nanofibers via a specific method can give compressible and elastic cellular aerogels with high pressure-sensitivity and good absorption/separation properties. [32,33] However, the limited bending flexibility and functionality of the aerogels are yet to be satisfactory. Moreover, the poor processability of traditional aerogels significantly restricts their practical applications. Therefore, a preparation of multifunctional aerogels combined with high mechanical properties including processability still remains a great challenge.

In our previous papers, it has been reported that controlled hydrolysis and condensation of trifunctional organoalkoxysilanes and organo-bridged alkoxysilanes can afford transparent nanoporous polyorganosilsesquioxane[34-36] and organo-briged polysiloxane[37,38] aerogels with good compressibility, elasticity, and thermal insulation properties. Moreover, an organic-inorganic double-cross-linking approach has been found to prepare transparent polyvinylpolymethylsiloxane (PVPMS), polyallypolymethylsiloxane (PAPMS), polyvinylpolysilsesquioxane (PVPSQ), and polyallypolysilsesquioxane (PAPSQ) aerogels with high flexibility, processability, and excellent thermal insulation properties. [39,40]

In this paper, we report unprecedented doubly cross-linked aerogels based on polyvinylpolydimethylsiloxane (PVPDMS) with excellent mechanical properties such as superflexiblity and processability and multifunctionality combining thermal insulation, selective absorption, and strain sensing properties via the double-cross-linking strategy consisting of free-radical polymerization/hydrolytic polycondensation without any additional organic cross-linkers. Free radical polymerization of a single precursor vinyldimethylmethoxysilane (VDMMS) or co-polymerization of precursors VDMMS and vinylmethyldimethoxysilane (VMDMS) in the presence of a radical initiator (di-tert-butyl peroxide, DTBP) is followed by hydrolytic polycondensation of the obtained polymers with a strong base catalyst (tetramethylammonium hydroxide, TMAOH) to give a doubly cross-linked porous structure consisting of flexible polydimethylsiloxanes (/polymethylsiloxanes) and

hydrocarbon chains. Aerogels based on the PVPDMS network and PVPDMS/polyvinylpolymethylsiloxane (PVPMS) copolymer network are then obtained via low-cost APD or FD. Highly flexible and conductive PVPDMS/PVPMS/graphene nanocomposite aerogels with a strain sensing property have also been prepared by a homogeneous incorporation of graphene nanoplatelets in the hydrolytic polycondensation process. Synthetic approaches toward an excellent combination of these functionalities in a single material system are discussed from the viewpoint of structure-property relationship.
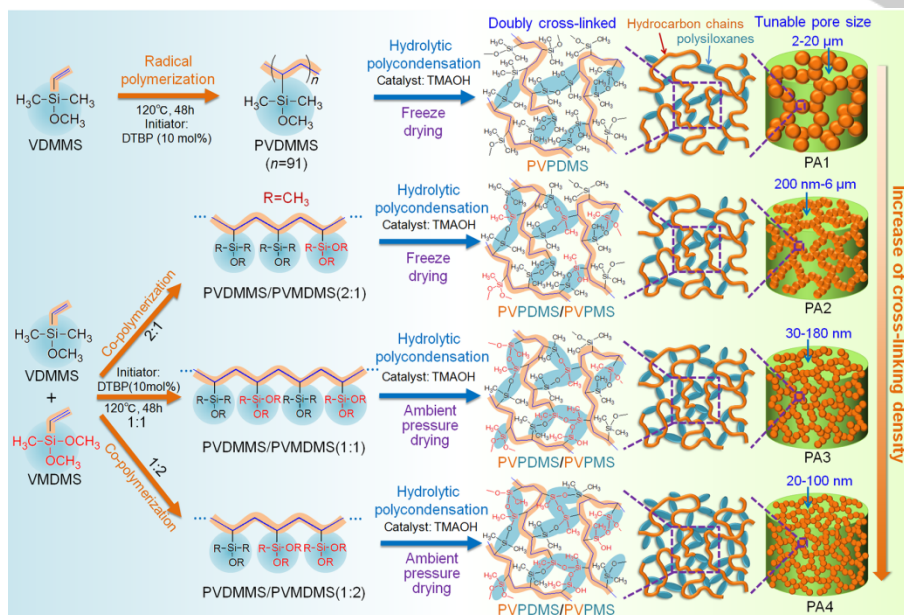

Figure 1. Schematic of facile synthesis of doubly cross-linked PVPDMS-based aerogels via the free-radical polymerization/hydrolytic polycondensation method.

Doubly cross-linked structure. The double cross-linking method for the preparation of PVPDMS-based aerogels is presented schematically in Figure 1. For all the samples, temperature, time, and the DTBP concentration in radical polymerization are fixed at 120 °C, 48 h, and 10 mol%, respectively. The results on the radical polymerization of VDMMS and co-polymerization of VDMMS and VMDMS with the molar ratio of 1:1 are shown in Table S1. The resulting PVDMMS and PVDMMS/PVMDMS polymers exhibit a high molecular weight of 10536 and 37515, respectively. The degree of polymerization (n) of PVDMMS is as high as 91. There is no peak or absorption band corresponding to vinyl groups observed in the ^{29}Si CP/MAS NMR (Figure 2a) or FTIR (Figure S1) spectra, indicating the high conversion of PVDMMS and PVDMMS/PVMDMS.

The doubly cross-linked structure of the resulting aerogels is evidenced by the NMR and FTIR spectra (Figure 2a and Figure S1). As shown in the NMR spectra, the peaks located at around 7.6 and 12.6 ppm correspond to M^1 $(CH_2CH(Si(CH_3)_2O_{1/2}))_n$ and M^0 species, [41] respectively, indicating the presence of polydimethylsiloxanes and aliphatic hydrocarbon chains in the PVPDMS-based aerogels. The broad peak located at around −21 ppm corresponds to D^2 $(CH_2CH(Si(CH_3)O_{2/2}))_n$ and D^1 species, [37] indicating the presence of polymethylsiloxanes and aliphatic hydrocarbon chains in PVPDMS/PVPMS composite aerogels PA2, PA3, and PA4. In addition, the peak corresponding to M^1 becomes smaller while that corresponding to D^2 becomes more intense with the decrease of the molar ratio of VDMMS to VMDMS in the precursors. This indicates that the doubly cross-linked structure contains less polydimethylsiloxanes and more polymethylsiloxanes with the increase of the amount of VMDMS in the precursors. As presented in the FTIR spectra, the absorption bands corresponding to C−H, Si−C, and Si−O−Si bonds indicate the presence of the aliphatic hydrocarbon chains and/or methyl groups and polysiloxanes of the PVPDMS-based aerogels. [7,42] The doubly cross-linked porous structure with abundant hydrophobic methyl groups and aliphatic hydrocarbon chains and only a small amount of −OH groups allows the resulting aerogels to exhibit high hydrophobicity (Figure S2), low density (tunable in the wide range of 20−200 mg cm^{-3}), and many other outstanding properties as discussed later.
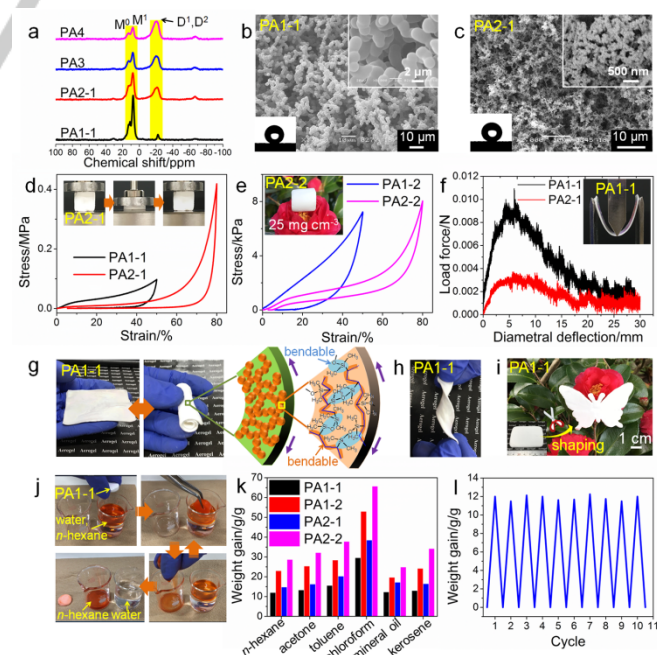
Figure 2. The microstructure, flexibility, processability, and absorption performance of typical PVPDMS-based aerogels. a) ^{29}Si CP/MAS NMR spectra of typical PVPDMS-based aerogels. b,c) SEM images of PA1−1 and

PA2−1. The insets of the SEM images present the contact angle of water of ~157°. d,e) Stress−strain curves of uniaxial compression−decompression tests on typical aerogels. The inset of d is the photograph of a uniaxial compression−decompression test on PA2−1. The inset of e is the photograph of PA2−2. f) Stress-strain curves of three-point bending tests on typical aerogels. g,h) hand bending and twisting tests on PA1−1. i) Excellent processability of a typical aerogel shown by shaping with a scissor. j) Photographs of n-hexane-water separation with PA1−1. k) Absorption capacities of typical aerogels for various organic solvents and oils. l) Absorption/drying cycle performance of PA1−1 for n-hexane.

**PVPDMS-based aerogels for absorption and separation.** Because the resulting PVDMMS molecules possess abundant hydrophobic groups and a relatively low concentration of hydrolyzable alkoxy groups, macroscopic phase separation between the hydrophobic condensates and polar solvent is induced during hydrolytic polycondensation.[35] Consequently, the PVPDMS aerogels PA1−1 and PA1−2 exhibit a randomly interconnected macroporous structure that consists of aggregated irregular spherical particles with a particle size in the range of 1.5−3 μm and a pore size in the range of 2−20 μm (Figure 2b and Figure S3). In the case of PVPDMS/PVPMS copolymer aerogels, the concentration of methyl groups is lower and that of hydrolyzable alkoxy groups is higher for the introduced PVMDMS molecules compared to those for PVDMMS molecules, which lead to higher cross-linking density and a lower tendency for the macroscopic phase separation. As a result, the composite aerogels PA2−1 and PA2−2 exhibit smaller sizes of particles (200−400 nm) and pores (200 nm−6 μm) as shown in Figure 2c and Figure S3. Due to the methyl- and hydrocarbon-rich doubly cross-linked structure, both PA1 and PA2 exhibit superhydrophobicity with a contact angle of water of ~157° (the inset of Figure 2b,c). Besides, these aerogels exhibit low density that is tunable in the wide range of 20−200 mg cm⁻³ (Table S2).

Because of their unique doubly cross-linked networks with flexible hydrocarbon chains and polydimethylsiloxanes (/polymethylsiloxanes), both the PVPDMS aerogels and PVPDMS/PVPMS copolymer aerogels PA2−1 and PA2−2 exhibit excellent mechanical properties. As shown in Figure 2d−f, the aerogels PA1−1, PA1−2, PA2−1, and PA2−2 exhibit high flexibility in both compression and bending. The PVPDMS aerogels (PA1−1 and PA1−2) are compressed with 50% strain without fracture and then recover nearly their original sizes, while the copolymer aerogels (PA2−1 and PA2−2) are compressed with 80% strain without fracture and then perfectly recover their original sizes after the force is removed. As we can see, the PVPDMS/PVPMS copolymer aerogels exhibit higher elasticity against compression compared to that of PVPDMS aerogels. This is probably because the polymethylsiloxanes with higher cross-linking density contribute to enhanced (or faster) relaxation after compression compared to that of the polydimethylsiloxanes with lower cross-linking density. Meanwhile, they recover nearly their original shapes from a large diametral deflection of 30 mm in the three-point bending tests with a fixture span of 25 mm without fracture. It is noteworthy that they can even be rolled up or twisted by hand without fracture (Figure 2g,h and Movie S1), showing superflexibility in bending and twisting. In addition, as shown in Figure 2i, these aerogels show excellent processability. A desired shape can be obtained simply by cutting with a scissor without fracture.

The combination of low density, highly porous structure, superhydrophobicity, superflexibility in compression and bending,

and excellent processability makes the resulting PVPDMS-based aerogels excellent absorption materials of organic solvents/oils for efficient oil-water separation. As a demonstration, PA1−1 is used for an *n*-hexane-water separation test (Figure 2j, Movie S2). Monolithic PA1−1 absorbs *n*-hexane quickly (with an absorption capacity of around 1200%) when it is placed in an *n*-hexane-water mixture, and the absorbed *n*-hexane can be easily squeezed out by hand. After several cycles, *n*-hexane can be completely separated from water with no damage observed in the aerogel. In addition to *n*-hexane, the PVPDMS-based aerogels can effectively absorb other organic solvents/oils such as acetone, toluene, chloroform, mineral oil, and kerosene. The absorption capacity, defined as weight of absorbed liquid per 1 g of aerogel, is varied in the range of 1200−6500% depending on the density of the solvents (Figure 2k). Furthermore, after immersing PVPDMS-based aerogels into *n*-hexane and drying at 60 °C for 10 cycles, the absorption capacity remains unchanged, showing an excellent absorption/drying cycle performance (Figure 2l). The absorption capacity of the PVPDMS-based aerogels is higher than those of the reported methyltrimethoxysilane (MTMS)−dimethyldimethoxysilane (DMDMS) gels (~120 mg cm⁻³) and vinyltrimethoxysilane (VTMS)−VMDMS gels due to the lower bulk density (25−94 mg cm⁻³).[7] Their absorption capacity is also higher than that of poly(vinyl alcohol)-based aerogels with the similar bulk density (25−85 mg cm⁻³) probably because they are more swollen and expand their volumes during absorption process.[28]
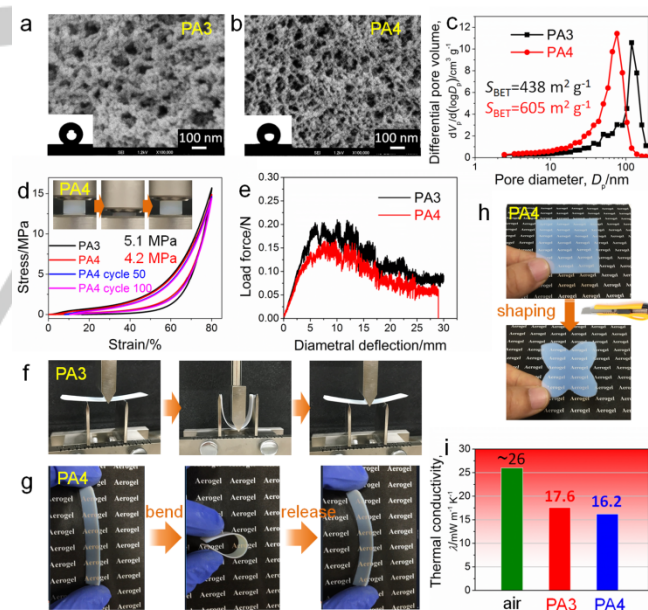
Figure 3. The pore structure, flexibility, processability, and thermal insulation performance of typical PVPDMS-based aerogels. a,b) SEM images of PA3 and PA4. The inset of the SEM image presents the contact angle of water of >140°. c) The BJH pore size distributions of PA3 and PA4. d) Stress-strain curves of uniaxial compression-decompression tests on typical aerogels and the compression cycle performance of PA4. The inset is the photograph of a uniaxial compression-decompression test on PA4. e) Stress-strain curves of three-point bending tests on typical aerogels. f) A three-point bending test on PA3. g) A hand bending test on PA4. h) Excellent processability of PA4 shown by shaping with a knife. i) Thermal conductivities of typical aerogels, showing a superinsulating performance.

PVPDMS-based aerogels for thermal superinsulation. When the amount of VMDMS in the precursors is further increased, PVPDMS-based copolymer aerogels with different microstructures and physical properties from those of PA1 and

PA2 can be obtained *via* APD. With the molar ratio of VDMMS to VMDMS decreasing to 1:1 and 1:2, the macroscopic phase separation is further suppressed by the network with lower hydrophobicity and higher cross-linking density, leading to a microstructure with smaller particle and pore sizes (Figure 3a-c and Figure S4). The particle and pore sizes of PA3 are 35−100 and 30−180 nm, respectively, while those of PA4 are 20−80 and 20−100 nm, respectively. Because of the abundance of nanosized particles and pores, PA3 and PA4 exhibit high SSAs of 438 and 605 m^2 g^{-1}, respectively. Due to homogeneity of the nanostructure, PA4 becomes even translucent with visible-light transmittance of 67% at wavelength of 550 nm for 1 mm thick sample (Figure 3h). Besides, since PA3 and PA4 are prepared from the precursors containing more VMDMS, which possesses more alkoxy groups and less methyl groups compared with those of VDMMS, more −OH groups (~3500 cm^{-1}) and less methyl groups (780 and 818 cm^{-1}) are observed in the FTIR spectra of PA3 and PA4 compared with those in PA2 and PA1 (Figure S1). Accordingly, the hydrophobicity of PA3 and PA4 becomes lower. In spite of this, the contact angles of water of PA3 and PA4 are still above 140° (150° and 142°, respectively, the inset of Figure 3a,b).

The aerogels PA3 and PA4 also exhibit excellent mechanical properties with high flexibility in both compression and bending. As presented in Figure 3d, both PA3 and PA4 are compressed with 80% strain without fracture and then perfectly and rapidly recover their original sizes after the force is removed. It should be noted that PA4 also recovers nearly its original size after compression–decompression with 80% strain for 100 cycles without fracture and with its porous microstructure unchanged (Figure 3d and Figure S5), indicating an excellent compression cycle performance. In addition, similar to the case of PA1 and PA2, PA3 and PA4 also recover nearly their original shapes from a large diametral deflection of around 30 mm in the three-point bending tests with a fixture span of 25 mm without fracture (Figure 3e,f). The hand bending tests clearly show the high bending flexibility of PA3 and PA4 (Figure 3g and Figure S6 and Movie S3). The bending flexibility of these aerogels is higher than that of the PVPMS aerogels with a similar bulk density in our previous work[39]. Furthermore, a desired shape can be obtained simply by cutting with a knife without fracture (Figure 3h), indicating the excellent processability of these aerogels.

Because of their moderately low density (0.19–0.20 g cm^{-3}) and small sizes of particles (20–100 nm) and pores (20–180 nm), the thermal conduction in the aerogels PA3 and PA4 is effectively suppressed. The measured thermal conductivities of PA3 and PA4 are as low as 17.6 and 16.2 mW m^{-1} K^{-1}, respectively, showing a thermal superinsulating performance (Figure 3i). These values are lower than those of stationary air (~26 mW m^{-1} K^{-1}),[30] nanocellulose (18–38 mW m^{-1} K^{-1})[30] and chitosan (22–30 mW m^{-1} K^{-1}) aerogels,[31] and commercial thermal insulation materials such as polyurethane foam (PUF, 20–50 mW m^{-1} K^{-1}) and mineral wool (35–80 mW m^{-1} K^{-1}),[14,39] and are comparable to those of silica (14–25 mW m^{-1} K^{-1}),[43,44] polymethylsilsesquioxane (PMSQ, 15–35 mW m^{-1} K^{-1}),[34,45] and PVPMS (15–16 mW m^{-1} K^{-1}) aerogels.[39] The low thermal conductivities, superflexibility, excellent processability together with the scalable APD will significantly contribute to their practical applications as flexible thermal superinsulators.

PVPDMS-based aerogels for strain sensing. In addition, the PVPDMS and PVPDMS/PVPMS aerogels can be further functionalized by incorporating conductive materials such as

graphene nanoplatelets to give highly flexible and conductive PVPDMS-based aerogels that can be applied as strain sensors. As a demonstration, conductive PVPDMS/PVPMS/graphene aerogels have been obtained by a simple hybridizing method (Figure 4a). Graphene nanoplatelets are first dispersed in benzyl alcohol and then subjected to ultrasonic agitation, after which the obtained suspension liquid was added to the PVDMMS/PVMDMS sol. The PVPDMS/PVPMS/graphene aerogels are obtained after sol-gel, aging, washing, and freeze drying. The resulting aerogel PA2–G exhibits superhydrophobicity with a contact angle of water of ~157°, the value of which is the same as that of PA2–1. The graphene nanoplatelets with 2–10 nm thickness and 5–15 µm width are well distributed in the highly porous aerogel matrix (Figure 4b). The PA2–G aerogel also shows excellent mechanical properties with high flexibility and elasticity against compression. It recovers nearly its original size after compression–decompression with 50% strain for 100 cycles without fracture (Figure 4c). Its porous microstructure remains unchanged after 100 cycles (Figure S7), indicating an excellent compression cycle performance.
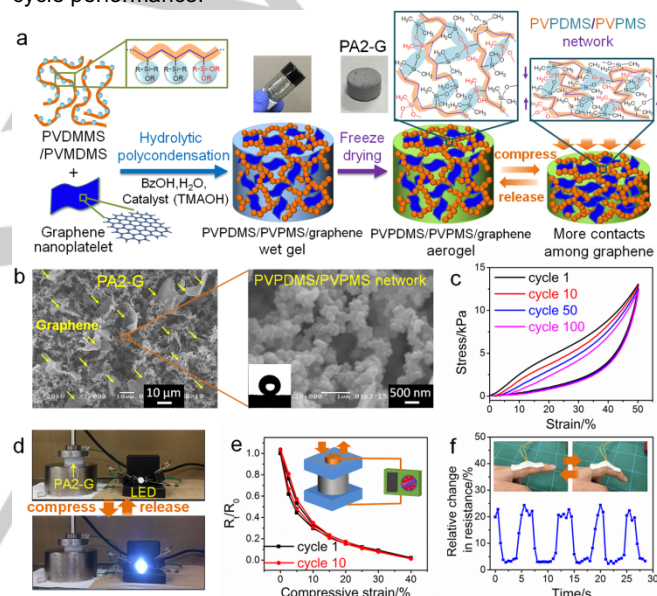
Figure 4. The schematic, pore structure, flexibility, and strain sensing performance of typical PVPDMS-based graphene composite aerogels. a) Schematic of synthesis of conductive PVPDMS/PVPMS/graphene aerogels. b) SEM images of PA2–G. The inset of the SEM image presents the contact angle of water of ~157°. c) 100 cycles of stress-strain curves of uniaxial compression-decompression tests on PA2–G. d) The brightness of a LED increases on compression of PA2–G and decreases after it is released. e) Normalized electrical resistance versus compressive strain for PA2–G. f) A strain sensor of PA2–G adhered to a finger.

Further, a light-emitting diode (LED) can be illumined by using a simple circuit connected with a cylindrical sample of PA2–G, indicating that the material is conductive (Figure 4d). It is noteworthy that the brightness fluctuates with compression and decompression of the aerogels (Figure 4d and Movie S4). Accordingly, the normalized electrical resistance decreases significantly with the increase of compressive strain in the range of 0–40%, and exhibits good recovery during the decompression process (Figure 4e). It decreases 97% at 40% strain, the value of which is higher than that of the aerogels based on nanofibers (<70% at 40% strain), indicating the high sensitivity of PA2–G against compressive strain.[32,33] The decrease of electrical resistance is because more contacts among graphene

nanoplatelets are produced upon compression, which increase the conduction paths. After compression-decompression with 40% strain for 10 cycles, the electrical resistance-strain curve remains nearly unchanged, indicating a good cycle performance. A strain sensor of PA2–G adhered to a finger is demonstrated additionally (Figure 4f). Relative changes in resistance versus time for finger bending are clearly detected, showing a strain sensing performance.

In conclusion, doubly cross-linked PVPDMS aerogels and their derivatives including PVPDMS/PVPMS copolymer and PVPDMS/PVPMS/graphene nanocomposite aerogels have been facilely prepared by a consecutive radical polymerization and hydrolytic polycondensation strategy from VDMMS or VDMMS/VMDMS, followed by low-cost ambient pressure drying or freeze drying. A unique doubly cross-linked organic-inorganic network structure consisting of flexible polydimethylsiloxanes (/polymethylsiloxanes) and hydrocarbon chains are obtained. The resulting PVPDMS-based aerogels exhibit tunable pore size (20 nm−20 µm), low density (tunable in the wide range of 20−200 mg cm^{-3}), high hydrophobicity (140−157° contact angle of water), excellent processability, superflexibility in both compression and bending, as well as mutifunctionality with a combination of efficient organic solvents/oils absorption and oil-water separation (1200−6500% absorption capacity), thermal superinsulation (λ=16.2−17.6 mW m^{-1} K^{-1}), and strain sensing. This study is expected to provide new concepts to synthesize multifunctional soft porous materials promising in the practical applications of absorbents, thermal superinsulators, sensors, wearable electronics, etc.

Acknowledgements

Conflict of Interests

The authors declare no conflict of interests.

Keywords: superflexible aerogel • multifunctional • absorbent • superinsulator • strain sensor

[1] N. Matsuhisa, D. Inoue, P. Zalar, H. Jin, Y. Matsuba, A. Itoh, T. Yokota, D. Hashizume, T. Someya, *Nature Mater.* **2017**, *16*, 834−840.

[2] T. Yamada, Y. Hayamizu, Y. Yamamoto, Y. Yomogida, A. Izadi-Najafabadi, D. N. Futaba, K. Hata, *Nature Nanotech.* **2011**, *6*, 296−301.

[3] D. Zhao, C. Chen, Q. Zhang, W. Chen, S. Liu, Q. Wang, Y. Liu, J. Li, H. Yu, *Adv. Energy Mater.* **2017**, *7*, 1700739−1700747.

[4] H. Chang, J. Qin, P. Xiao, Y. Yang, T. Zhang, Y. Ma, Y. Huang, Y. Chen, *Adv. Mater.* **2016**, *28*, 3504−3509.

[5] S. S. Kistler, *Nature* **1931**, *127*, 741.

[6] J. Fricke, *Nature* **1995**, *374*, 409−410.

[7] G. Hayase, K. Kanamori, M. Fukuchi, H. Kaji, K. Nakanishi, *Angew. Chem., Int. Ed.* **2013**, *52*, 1986−1989.

[8] Y. Huang, M. Zhong, F. Shi, X. Liu, Z. Tang, Y. Wang, Y. Huang, H. Hou, X. Xie, C. Zhi, *Angew. Chem., Int. Ed.* **2017**, *56*, 9141−9145.

[9] S. Chen, G. He, H. Hu, S. Jin, Y. Zhou, Y. He, S. He, F. Zhao, H. Hou, *Energy Environ. Sci.* **2013**, *6*, 2435−2439.

[10] D. B. Amabilino, D. K. Smith, J. W. Steed, *Chem. Soc. Rev.* **2017**, *46*, 2404−2420.

[11] H. B. Wu, X. W. Lou, *Sci. Adv.* **2017**, *3*, eaap9252.

[12] B. Lebeau, A. Galarneau, M. Linden, *Chem. Soc. Rev.* **2013**, *42*, 3661−3662.

[13] X. Lu, M. C. Arduini-Schuster, J. Kuhn, O. Nilsson, J. Fricke, R. W. Pekala, *Science* **1992**, *255*, 971−972.

[14] A. C. Pierre, G. M. Pajonk, *Chem. Rev.* **2002**, *102*, 4243−4265.

[15] J. L. Mohanan, I. U. Arachchige, S. L. Brock, *Science* **2015**, *307*, 397−400.

[16] N. Husing, U. Schubert, *Angew. Chem., Int. Ed.* **1998**, *37*, 22−45.

[17] G. Zu, J. Shen, W. Wang, L. Zou, Y. Lian, Z. Zhang, B. Liu, F. Zhang, *Chem. Mater.* **2014**, *26*, 5761−5772.

[18] G. Zu, J. Shen, L. Zou, W. Wang, Y. Lian, Z. Zhang, A. Du, *Chem. Mater.* **2013**, *25*, 4757−4764.

[19] Z. U. Khan, J. Edberg, M. M. Hamedi, R. Gabrielsson, H. Granberg, L. Wagberg, I. Engquist, M. Berggren, X. Crispin, *Adv. Mater.* **2016**, *28*, 4556−4562.

[20] M. Antonietti, N. Fechler, T. -P. Fellinger, *Chem. Mater.* **2014**, *26*, 196−210.

[21] A. E. Aliev, J. Oh, M. E. Kozlov, A. A. Kuznetsov, S. Fang, A. F. Fonseca, R. Ovalle, M. D. Lima, M. H. Haque, Y. N. Gartstein, M. Zhang, A. A. Zakhidov, R. H. Baughman, *Science* **2009**, *323*, 1575−1578.

[22] J. -Y. Hong, B. M. Bak, J. J. Wie, J. Kong, H. S. Park, *Adv. Funct. Mater.* **2015**, *25*, 1053−1062.

[23] S. S. Prakash, C. J. Brinker, A. J. Hurd, S. M. Rao, *Nature* **1995**, *374*, 439−443.

[24] Z. Wang, Z. Dai, J. Wu, N. Zhao, J. Xu, *Adv. Mater.* **2013**, *25*, 4494−4497.

[25] N. Leventis, *Acc. Chem. Res.* **2007**, *40*, 874−884.

[26] L. Jiang, K. Kato, K. Mayumi, H. Yokoyama, K. Ito, *ACS Macro Lett.* **2017**, *6*, 281−286.

[27] G. Hasegawa, T. Shimizu, K. Kanamori, A. Maeno, H. Kaji, K. Nakanishi, *Chem. Mater.* **2017**, *29*, 2122−2134.

[28] C. -B. Ma, B. Du, E. Wang, *Adv. Funct. Mater.* **2017**, *27*, 1604423−1604431.

[29] J. Wang, X. Zhang, *ACS Nano* **2015**, *9*, 11389−11397.

[30] Y. Kobayashi, T. Saito, A. Isogai, *Angew. Chem., Int. Ed.* **2014**, *53*, 10394−10397.

[31] S. Takeshita, S. Yoda, *Chem. Mater.* **2015**, *27*, 7569−7572.

[32] Y. Si, J. Yu, X. Tang, J. Ge, B. Ding, *Nat. Commun.* **2014**, *5*, 5802.

[33] Y. Si, Q. Fu, X. Wang, J. Zhu, J. Yu, G. Sun, B. Ding, *ACS Nano* **2015**, *9*, 3791−3799.

[34] G. Hayase, K. Kugimiya, M. Ogawa, Y. Kodera, K. Kanamori, K. Nakanishi, *J. Mater. Chem. A* **2014**, *2*, 6525−6531.

[35] K. Kanamori, M. Aizawa, K. Nakanishi, T. Hanada, *Adv. Mater.* **2007**, *19*, 1589−1593.

[36] T. Shimizu, K. Kanamori, A. Maeno, H. Kaji, C. M. Doherty, P. Falcaro, K. Nakanishi, *Chem. Mater.* **2016**, *28*, 6860−6868.

[37] T. Shimizu, K. Kanamori, A. Maeno, H. Kaji, K. Nakanishi, *Langmuir* **2016**, *32*, 13427−13434.

[38] T. Shimizu, K. Kanamori, A. Maeno, H. Kaji, C. M. Doherty, K. Nakanishi, *Langmuir* **2017**, *33*, 4543−4550.

[39] G. Zu, T. Shimizu, K. Kanamori, Y. Zhu, A. Maeno, H. Kaji, J. Shen, K. Nakanishi, *ACS Nano* **2018**, *12*, 521−532.

[40] G. Zu, K. Kanamori, T. Shimizu, Y. Zhu, A. Maeno, H. Kaji, K. Nakanishi, J. Shen, *Chem. Mater.* **2018**, *30*, 2759−2770.

[41] D. J. T. Hill, C. M. L. Preston, A. K. Whittaker, *Polymer* **2002**, *43*, 1051−1059.

[42] N. Moitra, S. Ichii, T. Kamei, K. Kanamori, Y. Zhu, K. Takeda, K. Nakanishi, T. Shimada, *J. Am. Chem. Soc.* **2014**, *136*, 11570−11573.

[43] L. Huber, S. Zhao, W. J. Malfait, S. Vares, M. M. Koebel, *Angew. Chem., Int. Ed.* **2017**, *56*, 4753−4756.

[44] J. C. H. Wong, H. Kaymak, S. Brunner, M. M. Koebel, *Microporous Mesoporous Mater.* **2014**, *183*, 23−29.

[45] G. Hayase, K. Kanamori, K. Abe, H. Yano, A. Maeno, H. Kaji, K. Nakanishi, *ACS Appl. Mater. Interfaces* **2014**, *6*, 9466−9471.

COMMUNICATION

Multifunctional doubly cross-linked aerogels: Highly flexible, processable, doubly cross-linked organic-inorganic hybrid aerogels are synthesized via a facile radical polymerization /hydrolytic polycondensation strategy. The obtained aerogels show multifunctionality with an excellent combination of selective absorption, efficient separation of oil and water, thermal superinsulation, and stain sensing.
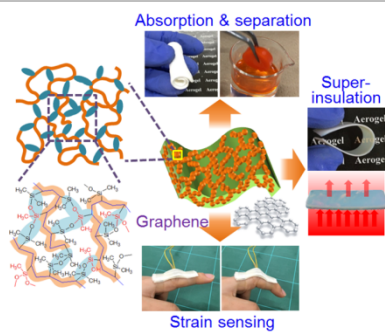
G. Zu, * K. Kanamori, * A. Maeno, H. Kaji, K. Nakanishi

Superflexible Multifunctional Polyvinylpolydimethylsiloxane-Based Aerogels as Efficient Absorbents, Thermal Superinsulators, and Strain Sensors

This PDF file includes:

Experimental section
Captions for Movies S1 to S4
Figures S1 to S7
Tables S1 and S2

Other Supplementary Materials for this manuscript include the following:

Movies S1 to S4

Experimental section

Materials. Vinyldimethylmethoxysilane (VDMMS) was purchased from Fluorochem Ltd (UK). Vinylmethyldimethoxysilane (VMDMS) and tetramethylammonium hydroxide (TMAOH, 25 wt % in water) were obtained from Sigma-Aldrich, Co. (USA). Graphene nanoplatelets with thickness × width of 2−10 nm × 5−15 μm and Di-*tert*-butyl peroxide (DTBP) were purchased from Tokyo Chemical Industry Co., Ltd. (Japan). 2-propanol (IPA), benzyl alcohol (BzOH), 2-methyl-2-propanol, and *n*-hexane were obtained from Kishida Chemical Co., Ltd. (Japan). Distilled water was purchased from Hayashi Pure Chemical Ind., Ltd. (Japan). All the chemical reagents were used as received.

Sample preparation. An appropriate amount of VDMMS (or VDMMS and VMDMS with the molar ratio of 2:1, 1:1, or 1:2) and DTBP (10 mol%) were mixed and charged in a hydrothermal reactor. After being flushed with Ar, the reactor was sealed and then heated at 120 °C for 48 h to promote free-radical polymerization of the precursors. A transparent and viscous liquid that mainly contains polyvinyldimethylmethoxysilane (PVDMMS) or PVDMMS/polyvinylmethyldimethoxysilane (PVMDMS) was obtained after cooling naturally at room temperature. For the PVPDMS and PVPDMS/PVPMS samples, BzOH, H_2O, and TMAOH aq. with specific molar ratios were added into the above solution in the listed order

under stirring. For the PVPDMS/PVPMS/graphene samples, a given amount of graphene nanoplatelets (30 wt% of the resulting aerogels) was dispersed in BzOH, then subjected to ultrasonic agitation for 1 h to afford a graphene suspension liquid, after which the obtained suspension and an appropriate amount of H_2O and TMAOH were added into the above polymerized precursors in the listed order under stirring. The mixture was stirred for 5 min, and then transferred into a container, which was then sealed and heated at 100 °C for 4 d to promote gelation and aging.

For freeze drying, the aged gel was washed with 2-methyl-2-propanol, and then frozen in a freezer and subjected to freeze drying at 40 Pa and −50 °C by a freeze dryer (FDU-12AS, Tokyo Rikakikai Co., Ltd., Japan) to obtain an aerogel. For ambient pressure drying, the gel was washed with IPA and *n*-hexane, followed by evaporation at room temperature for 2−4 d and at 80 °C for 4 h to obtain an aerogel.

Characterizations. Bulk density of aerogels was determined by measuring the height, diameter, and mass of cylindrical samples. The morphology was observed by a scanning electron microscope (SEM, JSM-6060S, JEOL, Japan) and a field emission scanning electron microscope (FESEM,JSM-6700F, JEOL, Japan). The chemical structures were investigated by a Fourier transform infrared (FTIR) spectroscope (IRAffinity-1, Shimadzu Corp., Japan). The ^{29}Si cross-polarization magic angle spinning (CP/MAS) nuclear magnetic resonance (NMR) measurements were conducted on an 800 MHz NMR spectrometer (Avance III 800US Plus, Bruker Corp., Germany) under the static magnetic field of 18.8 T. A double resonance probe with 4 mm MAS probe head was used. For all the samples, the MAS frequency was set to 12 kHz, contact time for CP process was 5.5 ms, the recycle delay was 4 s, and the number of scans was 4096. Hexamethylcyclotrisiloxane was used as an external reference material (the ^{29}Si chemical shift was set to −9.66 ppm). The N_2 adsorption-desorption isotherm, pore size distribution, and specific surface area were measured using a N_2 adsorption analyzer (BELSORP-mini, BEL Japan, Inc., Japan).The pore size distribution was obtained from the

adsorption branch by the Barrett−Joyner−Halenda (BJH) calculation. The specific surface area was derived from the Brunauer−Emmett−Teller (BET) method.

The weight-average molecular weight (M_w) and polydispersity (M_w/M_n) of PVDMMS and PVDMMS/PVMDMS were determined by a gel permeation chromatography (GPC) system (GPC104, Shodex, Japan) with a chloroform solvent and an LF604 column. The visible-light transmittance of the samples was measured by a UV−vis−NIR spectrophotometer (V-670, JASCO, Japan) equipped with an integrating sphere. Contact angles of water were measured using Drop Master (DM-561Hi, Kyowa Interface Science Co., Ltd., Japan) with the volume of the water droplet of 3 μL.

The uniaxial compression−decompression tests and three-point bending tests on aerogels were carried out using a material tester (EZGraph, Shimadzu Corp., Japan). The cross-head speed was 10 and 2 mm min^{-1} for compression and bending tests, respectively. A cylindrical aerogel with a diameter of 8−18 mm and a height of 4−14 mm was used for the compression tests. A sheet-shaped aerogel with typical width × length × thickness of 10 × 60 × 1 mm was used for the bending tests. The apparatus span in three-point bending tests was fixed at 25 mm.

Absorption capacity of the aerogels was calculated by equation $W = (M−M_0)/M_0$, where W is weight gain, M_0 is weight before absorption, and M is weight after saturated absorption. The samples were immersed into different solvents or oils. After being saturated, the samples were taken out and the residual liquid on surface was removed with a paper before each weight measurement. Absorption/drying cycle performance was studied by immersing aerogels into *n*-hexane and drying at 60 °C for 10 cycles.

The thermal conductivity of aerogels at room temperature and ambient pressure was measured using a heat flow meter (HFM 436 Lambda, NETZSCH, Germany). An aerogel plate with typical width × length × height of 100 × 100 × 10 mm was used.

Strain sensing performance (electrical resistance-strain curves) was studied by a material

tester (EZGraph, Shimadzu Corp., Japan) combined with an ohmmeter (M-04, Custom Corp., Japan) *via* a two-probe method. A cylindrical aerogel was loaded between two compression plates that were attached by copper wires to the ohmmeter for the resistance measurement.
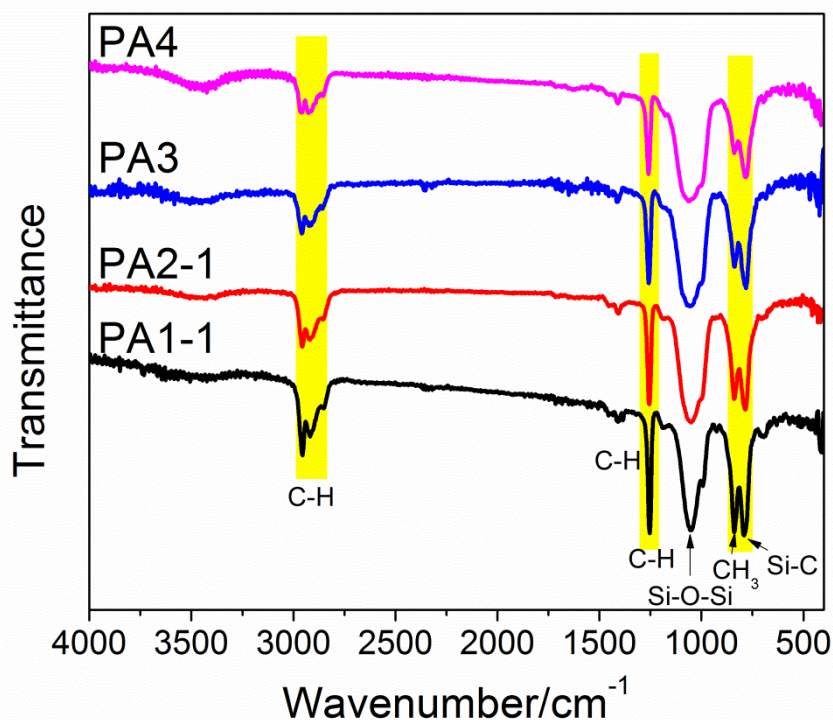
Movie list:

Movie S1. Superhydrophobicity and high bending flexibility of PA1-1.

Movie S2. Efficient *n*-hexane-water separation with PA1-1.

Movie S3. High bending flexibility of PA4 shown by hand bending.

**Movie S4**. Compression flexibility and strain-sensitive conductivity of PA2-G.

Figures:

Figure S1. FTIR spectra of typical PVPDMS-based aerogels. The absorption bands at ~1050 cm^{-1} are ascribed to the stretching of Si−O−Si bonds. The bands located at 2852 cm^{-1}, 2920 cm^{-1}, and 2957 cm^{-1} are attributed to the stretching of C−H bonds.[1-3] The bands at 780 cm^{-1},

~818 cm^{-1} and 1260 cm^{-1} correspond to the asymmetric stretching of Si−C bonds, rocking of CH$_3$ and asymmetric deformation of C−H bonds,[1] respectively. The Si−O−Si and Si−C bonds indicate the methyl-rich polydimethylsiloxanes and/or polymethylsiloxanes in the PVPDMS-based aerogels. The C−H and CH$_3$ bonds mainly result from the aliphatic hydrocarbon chains and methyl groups in the PVPDMS-based aerogels, respectively. Intensities of the C−H, CH$_3$, and Si−C bonds decrease with the decrease of the molar ratio of VDMMS to VMDMS in the precursors. This indicates that the doubly cross-linked structure contains less polydimethylsiloxanes and more polymethylsiloxanes with the increase of the amount of VMDMS in the preparation, which is consistent with the NMR results.
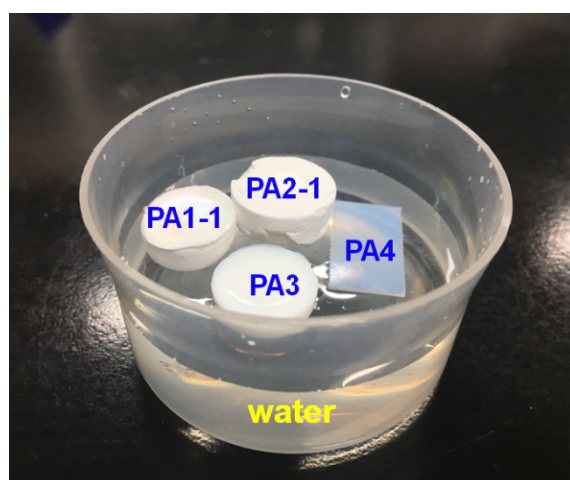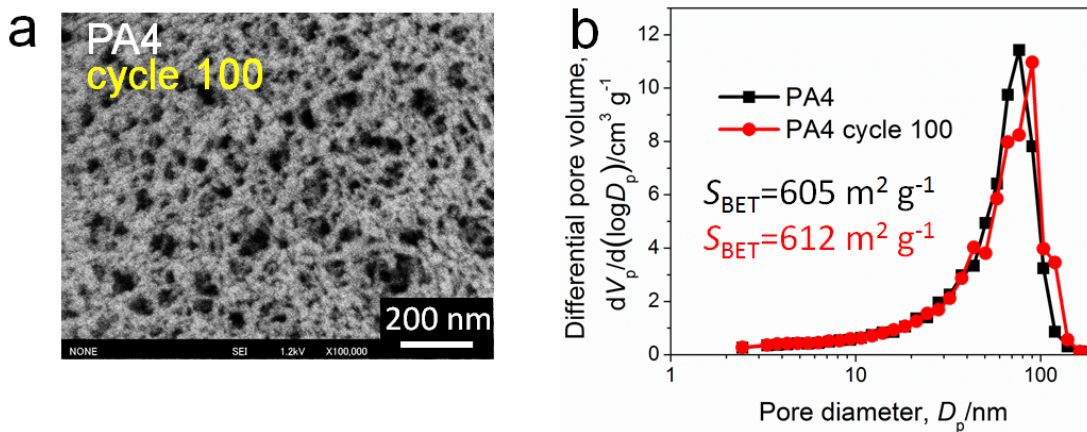

Figure S2. Contact of typical PVPDMS-based aerogels with water. All the samples float on top of water, showing high hydrophobicity.
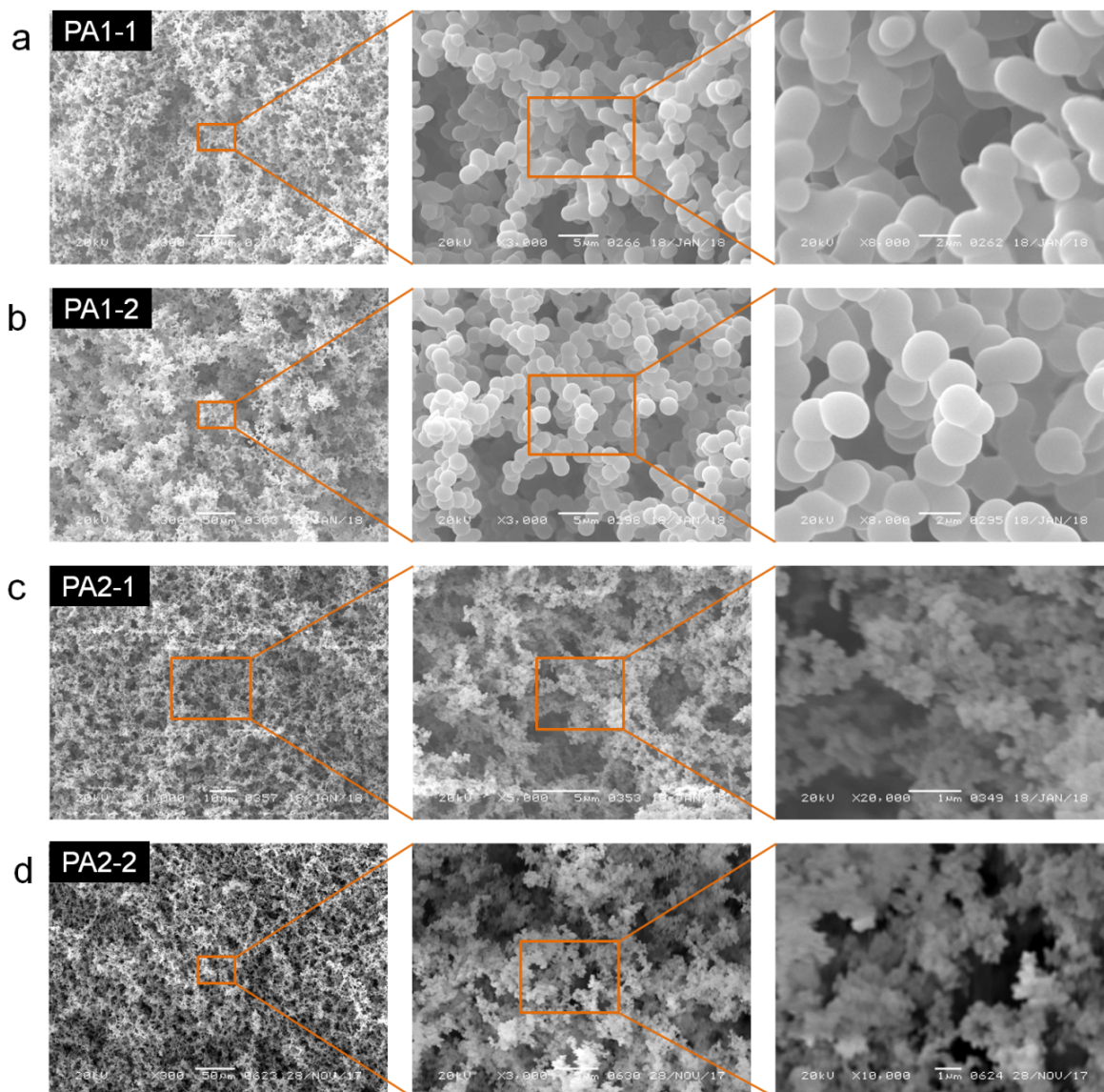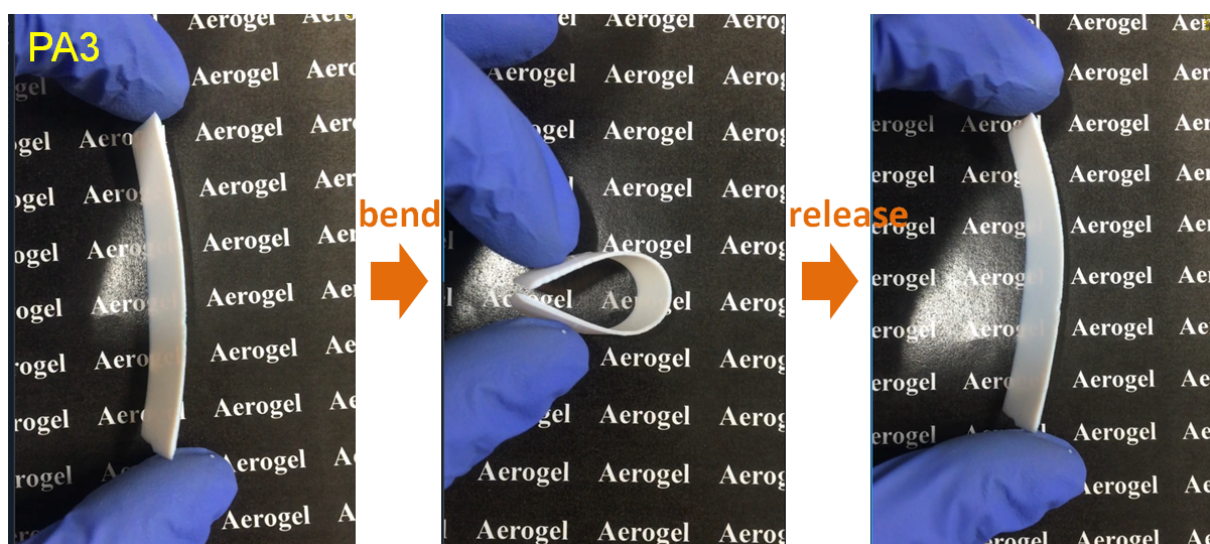
Figure S3. SEM images of typical PVPDMS-based aerogels (PA1-1, PA1-2, PA2-1, and PA2-2).
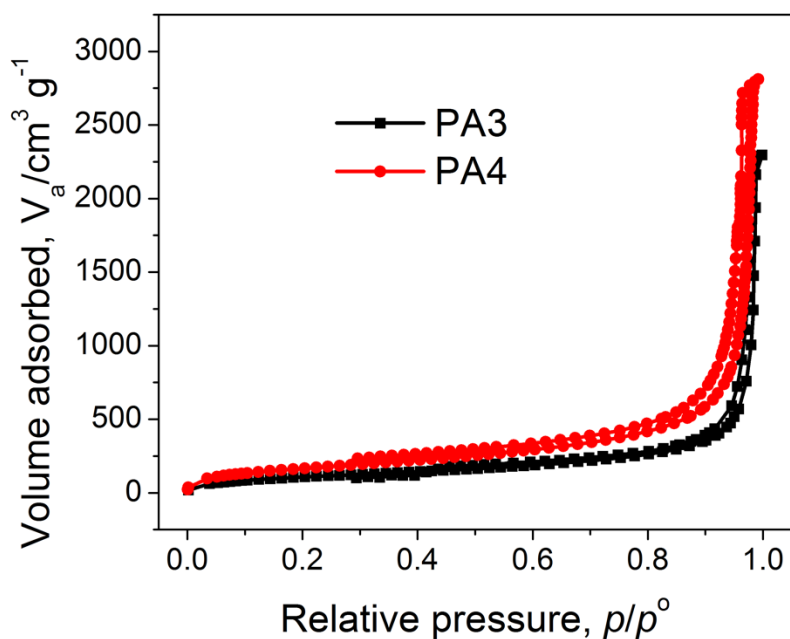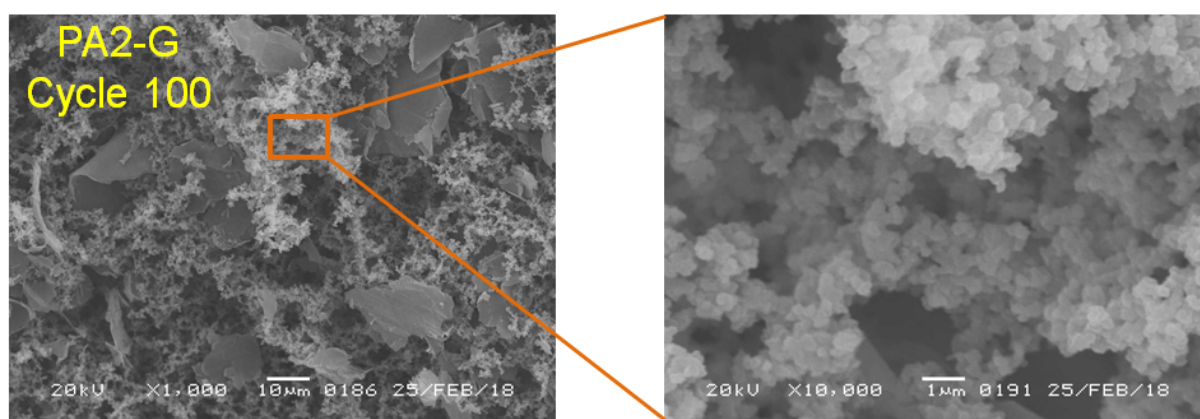
Figure S4. Nitrogen adsorption-desorption isotherms of PA3 and PA4.

Figure S5. a) Morphology and b) BJH pore size distribution of PA4 after compression-decompression with 80% strain for 100 cycles. It is found that its porous microstructure remains unchanged after 100 cycles.

Figure S6. High bending flexibility of PA3 shown by hand bending.

Figure S7. Morphology of PA2-G after compression-decompression with 50 % strain for 100 cycles. Its porous microstructure remains unchanged after 100 cycles.

Tables

Table S1. Results on the radical polymerization of VDMMS and co-polymerization of VDMMS and VMDMS with the molar ratio of VDMMS to VMDMS of 1:1.

Precursor	DTBP /mol%	Polymerization time /h	M_w	Degree of polymerization	M_w/M_n
VDMMS	10	48	10536	91	3.4
VDMMS/VMDMS	10	48	37515	302	8.45

Table S2. Starting compositions and physical properties of typical PVPDMS-based aerogels.

sample	VDMMS /mL	VMDMS /VDMMS /mol mol^{-1}	DTBP /mol%	BzOH/Si /mol mol^{-1}	H$_2$O/Si /mol mol^{-1}	TMAOH/Si /mol mol^{-1}	ρ[a] /mg cm^{-3}	S_{BET}[b] /m^2 g^{-1}	d[c] /nm
PA1-1	1	0	10	7.0	1.84	0.12	94	-	-
PA1-2	1	0	10	14.0	3.1	0.20	38	-	-
PA2-1	1	0.5	10	13.0	1.64	0.11	54	-	-
PA2-2	1	0.5	10	26.0	3.3	0.22	25	-	-
PA3	1	1	10	4.4	1.5	0.10	200	482	103
PA4	1	2	10	4.3	1.67	0.10	190	605	76

[a] Bulk density. [b] Brunauer-Emmett-Teller (BET) SSA obtained from nitrogen adsorption measurement. [c] Mean pore diameter obtained from nitrogen adsorption branch via the Barrett-Joyner-Halenda (BJH) method.

References

1. Hayase, G.; Kanamori, K.; Fukuchi, M.; Kaji, H.; Nakanishi, K. Facile Synthesis of Marshmallow-like Macroporous Gels Usable under Harsh Conditions for the Separation of Oil and Water. *Angew. Chem., Int. Ed.* **2013**, *52*, 1986-1989.
2. Hong, J. Y.; Bak, B. M.; Wie, J. J.; Kong, J.; Park, H. S. Reversibly Compressible, Highly Elastic, and Durable Graphene Aerogels for Energy Storage Devices under Limiting Conditions. *Adv. Funct. Mater.* **2015**, *25*, 1053-1062.
3. Moitra, N.; Ichii, S.; Kamei, T.; Kanamori, K.; Zhu, Y.; Takeda, K.; Nakanishi, K.; Shimada, T. Surface Functionalization of Silica by Si−H Activation of Hydrosilanes. *J. Am. Chem. Soc.* **2014**, *136*, 11570-11573.